Journal of Dentistry 163 (2025) 106196

Contents lists available at ScienceDirect

Journal of Dentistry

journal homepage: www.elsevier.com/locate/jdent

Nano-structural reinforcement of glass ionomer cement: unleashing the potential of hydroxyapatite and tetracalcium phosphate

Nozimjon Tuygunov [b,j], Azwatee Abdul Aziz [c], Arief Cahyanto [d,e], Bakhtinur Khudanov [a,b], Muhammad Aidil Roslan [f], Zamri Radzi [g], James Tsoi [h,i], Noor Azlin Yahya [c,*]

[a] Impulse Medical Institute, Tashkent region, Uzbekistan
[b] Department of Preventive Dentistry, Tashkent State Medical University, 100047, Tashkent, Uzbekistan
[c] Department of Restorative Dentistry, Faculty of Dentistry, Universiti Malaya, Kuala Lumpur 50603, Malaysia
[d] Department of Clinical Sciences, College of Dentistry, Ajman University, Ajman P.O. Box 346, United Arab Emirates
[e] Centre of Medical and Bio-allied Health Sciences Research, Ajman University, Ajman P.O. Box 346, United Arab Emirates
[f] Department of Science and Technology Studies, Faculty of Science, Universiti Malaya, Kuala Lumpur 50603, Malaysia
[g] Department of Orthodontics, Pediatric and Special Care Dentistry, Faculty of Dentistry, Universiti Malaya, Kuala Lumpur 50603, Malaysia
[h] Dental Materials Science, Faculty of Dentistry, The University of Hong Kong, Hong Kong SAR, China
[i] Center of Excellence in Precision Medicine and Digital Health, Department of Physiology, Faculty of Dentistry, Chulalongkorn University, Bangkok 10330, Thailand
[j] Department of Restorative Dentistry, Kimyo International University in Tashkent, Tashkent, 100001, Uzbekistan

ARTICLE INFO

Keywords:
Glass ionomer cement
Hydroxyapatite
Tetracalcium phosphate
Bioactivity
Biomaterials
Mechanical strength

ABSTRACT

Objective: To investigate the effects of hydroxyapatite (HAP) and tetracalcium phosphate (TTCP) addition into fabricated nano-sized GIC.

Methods: Seven groups were evaluated in this study. Group A, consisting of commercially available GIC served as control group, while the remaining six groups (Groups B-G) comprised fabricated GIC associated with different ratio of HAP and TTCP. Chemical characterization was performed using FE-SEM, EDX, XRD, and FTIR. Physio-mechanical assessment included particle size distribution (PSD), initial setting time, ions release (F^-, Ca^{2+}, PO_4^{3-}), pH measurement, and compressive strength. Statistical analyses were performed using one-way and repeated measures ANOVA, followed by post-hoc tests ($p < 0.05$).

Results: The fabricated nano-sized GIC powder exhibited an amorphous phase, confirmed through XRD and FTIR analyses, and achieved a significantly reduced particle size of 92.2 ± 2.69 nm, compared to 769.3 nm in control group. Incorporating TTCP extended the setting time, particularly at 570 seconds longer than the control group, while HAP reduced it by up to 422 seconds. Calcium ion release was significantly enhanced in TTCP-modified GIC, with Group C (10 % TTCP; 0 % HAP) showing the highest release (2.4 ppm), while HAP-modified GICs demonstrated significantly improved compressive strength, reaching up to 112.25 ± 4.80 MPa in Group G (0 % TTCP; 10 % HAP). Fluoride ion release was consistent across all experimental groups, peaking on the first day and gradually decreasing over 28 days. The addition of TTCP and HAP shifted the pH of GICs from acidic (pH ~1.0) to neutral (pH ~6.9).

Conclusions: The incorporation of TTCP and HAP into the fabricated GIC enhanced ion release and adjusted pH, showing potential advantages for dental applications. Further investigations are needed to explore their clinical relevance and long-term performance.

Clinical significance: This study highlights that TTCP additions significantly enhance calcium/phosphate ion release and shift pH toward neutrality, whereas HAP-modified GICs improve compressive strength to levels meeting restorative standards. However, TTCP-modified GICs exhibit prolonged setting times and notably reduced compressive strength, limiting their suitability for load-bearing restorations; they are better positioned as liners/bases or for non–load-bearing, remineralization-oriented applications where bioactivity is prioritized over mechanical performance.

* Corresponding author.
E-mail address: nazlin@um.edu.my (N.A. Yahya).

https://doi.org/10.1016/j.jdent.2025.106196
Received 4 June 2025; Received in revised form 6 October 2025; Accepted 22 October 2025
Available online 24 October 2025

1. Introduction

Over the past decades, conventional GIC has been widely used in dentistry due to its advantageous physical, chemical, and anticariogenic properties compared to water-based cements [1]. Notably, its fluoride ion release and commendable bioactivity make it a preferred choice for dental applications [1,2].

However, conventional GICs exhibit several limitations, including their weak bonding between tooth structures [3]. Enhancing this bonding can be achieved imparting genuine bioactive properties, such as promoting the formation of an apatite interlayer through increased Ca^{2+} and PO_4^{3-} ion release [4,5]. The deposition of apatite on the GIC surface could bridge gap between the restoration and tooth, strengthen adhesion, and improve tooth integration [6]. Despite these potential benefits, conventional GICs face challenges in forming an apatite. This is due to the release of polyacrylic acid, which reduces the pH and inhibits apatite formation [7]. Hence, there is a need to formulate bioactive GIC that has the capability of augmenting Ca and PO_4 ion release, thereby facilitating the formation of hydroxyapatite on their surface. Another limitation of GIC is its relatively low mechanical strength. Various alterations to either the liquid or glass powder components have been explored to enhance its mechanical properties [8,9]. These alterations led to an imbalance in specific properties, where enhancement in mechanical strength is associated with a simultaneous decline in other properties, thereby affecting the overall performance of the material [10,11].

With a calcium-to-phosphorus atomic ratio of 1.67, hydroxyapatite (HAP), is the most stable and least soluble form of calcium phosphate found in nature [8]. Due to its remarkable biocompatibility potential, HAP has been extensively used in a wide range of biomedical applications, including implant coatings, bone scaffolds, bone fillers, and drug delivery systems [10]. The incorporation of HAP into conventional GIC has enhanced its mechanical properties in terms of compressive strength, flexural strength, tensile strength, shear bond strength, fracture toughness, and microhardness [12]. Given its structural similarities to the mineral component of natural teeth, HAP contributes to the reinforcement of GIC resulting to the improvement of its mechanical performance and clinical efficacy [12].

On the other hand, tetracalcium phosphate (TTCP) is the only calcium phosphate compound with a Ca/P ratio higher than HAP [13]. It was found that TTCP improves dentine bridge formation without causing inflammation or necrosis in pulp tissue [14]. When incorporated in composite materials, TTCP has been shown to markedly increase the release of Ca^{2+} and PO_4^{3-} ions, particularly in acidic environments associated with cariogenic activity. The enhanced ion release is considered a key factor in its potential use as a dental restorative material [15]. Besides, TTCP exhibits superior biocompatibility, when used as a root canal sealant. Considering its chemical similarity to HAP, a mineral component of natural teeth, TTCP is able to promote bone and tissue growth [16].

In addition to that, several cell culture studies have confirmed high biocompatibility of TTCP scaffolds, demonstrating their ability to support cell growth, proliferation, and attachment, making them a promising material for various medical and dental applications [17]. TTCP has also shown potential in remineralization strategies, as its addition in chewing gum formulations has been reported to enhance mineral supersaturation levels, potentially aiding in the prevention of dental caries [18].

Given the limitations of conventional GICs and the promising properties of HAP and TTCP, there is a need to develop a bioactive, mechanically reinforced GIC with enhanced ion release. Thus, this study aims to fabricate a nano-sized GIC powder modified with TTCP and HAP to improve ion release, structural integrity, and durability, contributing to the advancement of high-performance restorative dental materials.

2. Materials and methods

2.1. Fabrication of nano-GIC powder

The GIC powder was fabricated using the melt-quenching method. Chemicals with weight compositions of 45 % silicon dioxide (SiO_2), 35 % aluminium oxide (Al_2O_3), 15 % calcium difluoride (CaF), 3 % phosphorus pentoxide (P_2O_5), and 2 % calcium oxide (all from Sigma-Aldrich, Germany) were weighed using an electronic balancer (JS1203C, Mettled Toledo, Switzerland). The resulting mixture was placed in a ceramic crucible and heated to 1250 °C for 2 hrs at a rate of 10 °C/min using an electric furnace (XY-1700, Xinkyo, Henan, China). The obtained glass frits were incubated at 40 °C for 24 hrs before being crushed to obtain fluoroaluminosilicate glass powder.

Fabricated GIC powders were processed by a two-step dry planetary ball-milling protocol. After initial deagglomeration, powders were passed through a 106 μm stainless-steel sieve (Endecotts, UK). Fraction <106 μm was loaded into a zirconia (ZrO_2) jar (50 mL) with 1.0 mm ZrO_2 balls at a powder:ball mass ratio of 1:10. Milling was performed at 300 rpm for 2 hrs using a planetary mill (Emax, Retsch, Germany) with intermittent cycles (15 mins on / 5 mins off) to limit heat buildup; jar temperature was kept <40 °C. Jars and media were pre-cleaned with ethanol and dried to minimize cross-contamination; milling was conducted under low humidity to reduce static. An aliquot was withdrawn for interim PSD. For the second stage, the residue was milled with 0.5 mm ZrO_2 balls (same jar, 1:10 mass ratio) at 300 rpm for an additional 2 hrs using the same duty cycle. Post-milling, powders were gently disaggregated with an agate spatula (no grinding) and re-sieved at 106 μm to remove any coarse fragments. Samples were stored in sealed, desiccated containers (silica gel) until analysis.

The GIC samples were divided into seven groups, each with different ratios of hydroxyapatite (HAP) and tetracalcium phosphate (TTCP) (Table 1). Group A used conventional GIC (Riva Self Cure Powder/Liquid Kit, Australia) and served as the control group. The remaining groups had HAP and TTCP incorporated using a multipurpose grinder (Bear Electric Appliance Co., Shunde, China) for 1 min to ensure uniform blending with consistent force, speed, and time. In accordance with the manufacturer's guidelines, the particle size of HAP (Sigma-Aldrich, Germany) was specified as 5 μm, whereas TTCP (Taihei Chemical Industrial, Japan) exhibited a particle size of <100 nm.

The powder-to-liquid ratio (PLR) was standardized at 3:1 for all groups following manufacturer's recommendation. All specimens were prepared using the conventional GIC liquid (Riva Self-Cure SDI Ltd., Victoria, Australia) at room temperature. The incorporation of TTCP and HAP in the experimental groups was done using a multipurpose grinder with a consistent force, speed, and time to ensure uniform blending.

2.2. Sample size calculation

For physical analysis in this study, initial setting time, pH and F, Ca and P ion values were determined by preparing three specimens for each formulation and three separate pH [19], F [20], Ca [21] and P ions release [15] readings were recorded for each specimen reference. The sample size for the mechanical strength analysis, specifically the compressive strength test, was determined using the G*Power software (version 3.1). The minimum number for sample size was 10 specimens in each group. The sample was calculated based on formulations that has been establihsed in a previous study [18]. The significance level was set at $p < 0.05$, the power sample size was more than 80 % in this study, and the confidence interval was 95 %.

2.3. Chemical characterization of GIC

2.3.1. FE-SEM and EDX analysis

Field emission scanning electron microscope (FE-SEM) (JEOL JSM-7900F, Tokyo, Japan) with attached UltiMax 170 mm^2 Energy

dispersive X-ray (EDX) detector (Oxford Instruments, Abingdon, UK) was employed to characterize chemical compounds of the prepared samples. Samples from each group were analyzed at 3000×, 5000×, 16000×, and 120000× magnifications on three separate locations to observe nanoscale features and additives.

The Ca/P ratio for each sample was determined using EDX analysis. Such analysis was conducted three times on different sections of the sample to ensure data consistency and sample variability. Atomic percentages of Ca and P were measured at multiple spots on each sample. The Ca/P ratio was calculated based on following equation:

$$Ca \Big/ P\ ratio = \frac{molar\ \%\ of\ Ca}{molar\ \%\ of\ P}$$

2.3.2. XRD analysis

Characterization of crystalline material was done using an X-ray diffractometry (Panalytical X'Pert Pro, Almelo, Netherlands). In this study, the XRD patterns was measured and scanned between 2θ (5-90°) with a step size of 0.05° in continuous mode at 25 °C and a counting time of 2 s per step. The generated data were analyzed using OriginLab software (OriginLab Corp., Northampton, MA, USA), with the use of the JCPDS-ICCD (Joint Committee on Powder Diffraction Standards-International Centre for Diffraction Data) files as references for the interpretation of the XRD patterns provided by each sample.

2.3.3. FTIR analysis

Fourier-transform infrared spectroscopy (FITR) (Nicolet 6700 FTIR spectrometer, Thermo Fisher Scientific, Waltham, MA, USA) was used to verify the XRD patterns and to identify the structural groups of the prepared composites. FTIR spectra were acquired in the wavenumber range of 4000-650 cm^{-1} at room temperature and a resolution of 0.5 cm^{-1}. Ethanol was applied to clean the surface to prevent cross contamination between samples.

2.4. Physio-mechanical characterization of GIC

2.4.1. PSD analysis

A particle size analyzer (Zetasizer Nano, Malvern Panalytical, Malvern, UK) was used to measure the particle size distribution (PSD) of the prepared samples. During the process, the measurement of each sample was replicated three times to ensure the reliability and consistency of the results. Thus, the average PSD was calculated using following equation:

$$\textbf{Average PSD} = \frac{(avarage\ size\ Peak\ 1 * intensity\ Peak\ 1) + (avarage\ size\ Peak\ 2 * intensity\ Peak\ 2) + (avarage\ size\ Peak\ 3 * intensity\ Peak\ 3)}{100\%}$$

2.4.2. Initial setting time

The setting times of each cement (n=3) were measured using a Vicat apparatus (NL Scientific, Selangor, Malaysia) in accordance with ISO 9917 standards [22]. The Vicat indenter is 400 ± 5 g in weight, with a needle having a flat end of 1.0 ± 0.1 mm in diameter. A mold with internal cross-sectional dimensions of 10 × 8 mm^2 was filled with the prepared cement mixture. Sixty seconds after mixing, the cement samples were incubated in an oven at 37 °C. To determine the appropriate setting time, the indentation was repeated at 30 s intervals until the needle failed to make a complete circular indentation in the cement [23].

2.4.3. Fluoride, calcium, and phosphate ions release

To assess F ion release, specimens (n=3) of each material were prepared using cylindrical Teflon molds with a diameter of 6 mm and a thickness of 4 mm. The cement was mixed and inserted into the mold for each specimen, then covered with a mixing pad on the top and bottom surfaces and compressed. Following an initial setting time of 1 hr, each specimen was individually immersed in a container with 5 mL of deionized water and stored at 37 °C under 100 % humidity for 24 hrs. The F release was measured after 1, 3, 6, 12, and 24 hrs and after 3, 7, 14, and 28 days using a pH/ion meter (SevenDirect SD50, Metler Toledo, China). Prior to the analysis, 1 mL of the solution was mixed with 1 mL of TISAB III (Thermo Fisher Scientific, Waltham, MA, USA), and the process was duplicated. Following each measurement, the machine was calibrated using F standards (Cole Parmer, Vernon Hills, IL, USA) at 0.1, 1, 10, and 100 ppm.

To assess Ca ion release, specimens (n=3) of each group were prepared using cylindrical Teflon molds with a diameter of 6 mm and a thickness of 4 mm. The cement was mixed and inserted into the mold for each specimen, subsequently covered with a mixing pad on the top and bottom surfaces, and compressed. After an initial setting period of 1 hr, each specimen was individually immersed in acrylic bottles containing 5 mL of deionized water and stored at 37 °C under 100 % humidity for 24 hrs. Calcium ion release was measured using atomic absorption spectroscopy (Perkin Elmer, Waltham, MA, USA). Following the storage period, calcium concentration was determined by acidifying 1 ml of the sample solution with 0.5 mL of 1 M HCl, followed by dilution with 0.5 mL of 2 % lanthanum chloride. The measurements were compared with a calibration curve of seven calcium standards ranging from 0 to 100 ppm. The Ca release of each specimen was measured after 1, 3, 6, 12, and 24 hours and after 3, 7, 14, and 28 days.

Prior to the evaluation of P ion release, samples (n=3) from each group were prepared, with each having a diameter of 6 mm and a thickness of 4 mm. The cement was mixed and placed into a mold, and subsequently compressed and covered with a mixing pad on both top and bottom surfaces. After an initial setting time of 1 hr, each specimen was separately immersed in 100 mL of deionized water and maintained at a constant temperature of 37 °C under humidity of 100 % for 24 hrs.

For quantification of P ion concentration, a sample solution was mixed with 500 mL of a 4.2 % ammonium molybdate solution. Following this, 20 mL of 1.5 % TWEEN 20 was added d to the mixture. The P ions concentration in the resulting solution was then quantified via colorimetric methods using a UV-Vis spectrophotometer (Shimadzu Corp., Kyoto, Japan). The results were compared with a calibration curve of

Table 1
Different amount of HAP and TTCP incorporated into fabricated nano-sized GIC among seven groups (weight %).

Tested materials	Group A	Group B	Group C	Group D	Group E	Group F	Group G
Fabricated GIC	Conventional GIC	100	90	90	90	90	90
TTCP		0	10	7	5	3	0
HAP		0	0	3	5	7	10

seven P standard solutions ranging from 0 to 100 ppm.

2.4.4. pH measurement

The pH measurement was conducted in accordance with ISO standards [24]. Test materials (n=3) were mixed and placed in a circular Teflon mold with the measurement of 6 mm in inner diameter and 4 mm in height. The molds were then compressed between the mixing pad to remove excess material. After 30 mins, the specimens were removed from the molds and placed in 100 mL sterile, hermetically sealed polyethylene containers. Five ml of deionized water was added into each container and the samples were incubated at 37 °C. A pH meter (Eutech pH700, Hanoi, Vietnam) was used to measure pH changes by immersing it into the central portion of the solution. The electrode was rinsed between measurements. All pH readings were recorded twice at the following interval times—1, 3, 6, 12 and 24 hrs as well as 3, 7, 14, and 28 days post specimen preparation—and the average pH reading for each sample was calculated.

2.4.5. Compressive strength analysis

Compressive strength test was determined in accordance with ISO 9917 requirements [24]. Cylindrical specimens (n=10) were prepared using PPTF Teflon molds (Chemours, Wilmington, DE, USA) with a measurement of 4 mm and 6 mm in height. The molds were filled with the material, compressed between mixing paper pads, flattened, and

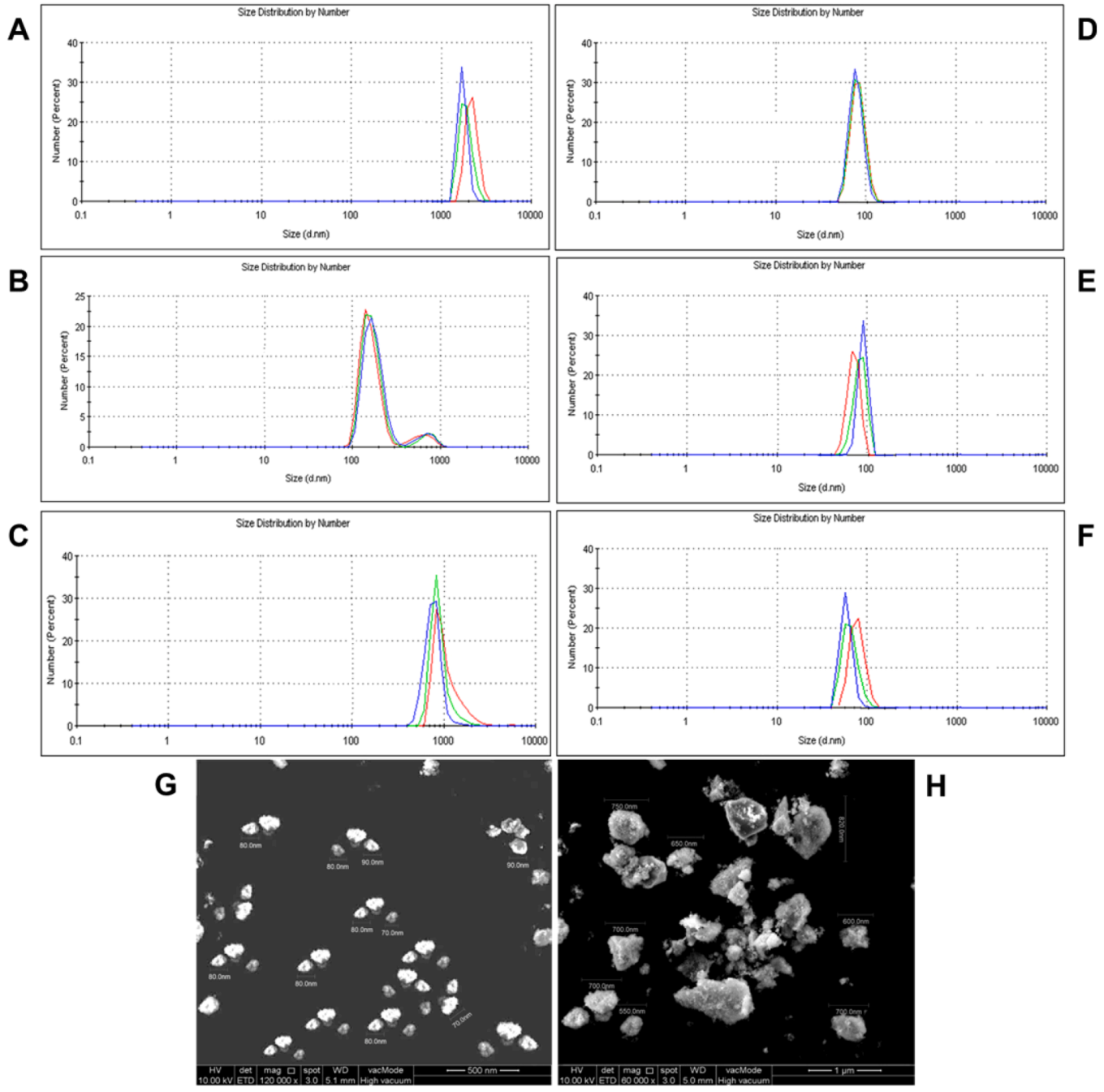

Fig. 1. PSD and FESEM Analysis of Fabricated and Conventional GIC. A: Manual crushing resulted in particles with an average size of 1855 nm. B: First-stage milling reduced the particle size to 224.2 nm for 90.7 % of the samples and 702.4 nm for the remaining 9.3 % samples. C: Commercial GIC showed an average particle size of 769.3 nm. D–F: Second-stage milling of the fabricated GIC reduced the particle size to 92.2 ± 2.69 nm. G: FESEM of the fabricated GIC exhibited an average particle size of 80.0 ± 6.32 nm. H: FESEM of the commercialized GIC demonstrated an average particle size of 683.75 ± 78.88 nm.

gently pressed by hand to remove air bubbles, before being clipped. The specimens were subsequently incubated at 37 °C under 100 % humidity for 24 hrs. Compressive strength test was performed using a universal testing machine (AGS-X Series Shimadzu, Kyoto, Japan) equipped with a 10 kN load cell and a crosshead speed of 10 mm/min. Cylindrical specimens (4 ± 0.1 mm in diameter and 6 ± 0.1 mm in height) were prepared following ASTM D695 standards. After being removed from the mold, the dimensions of each specimen were verified using a digital caliper (Mitutoyo, Kanagawa, Japan). The compressive strength (C) was calculated in megapascals (MPa) according following equation:

$$C = 4P/\pi D^2$$

Where, P (N) is the maximum load and D (mm) is the diameter of the specimen. The test was replicated 10 times for each material [25].

2.5. Statistical analysis

Data were recorded and analyzed with SPSS Statistics for Windows

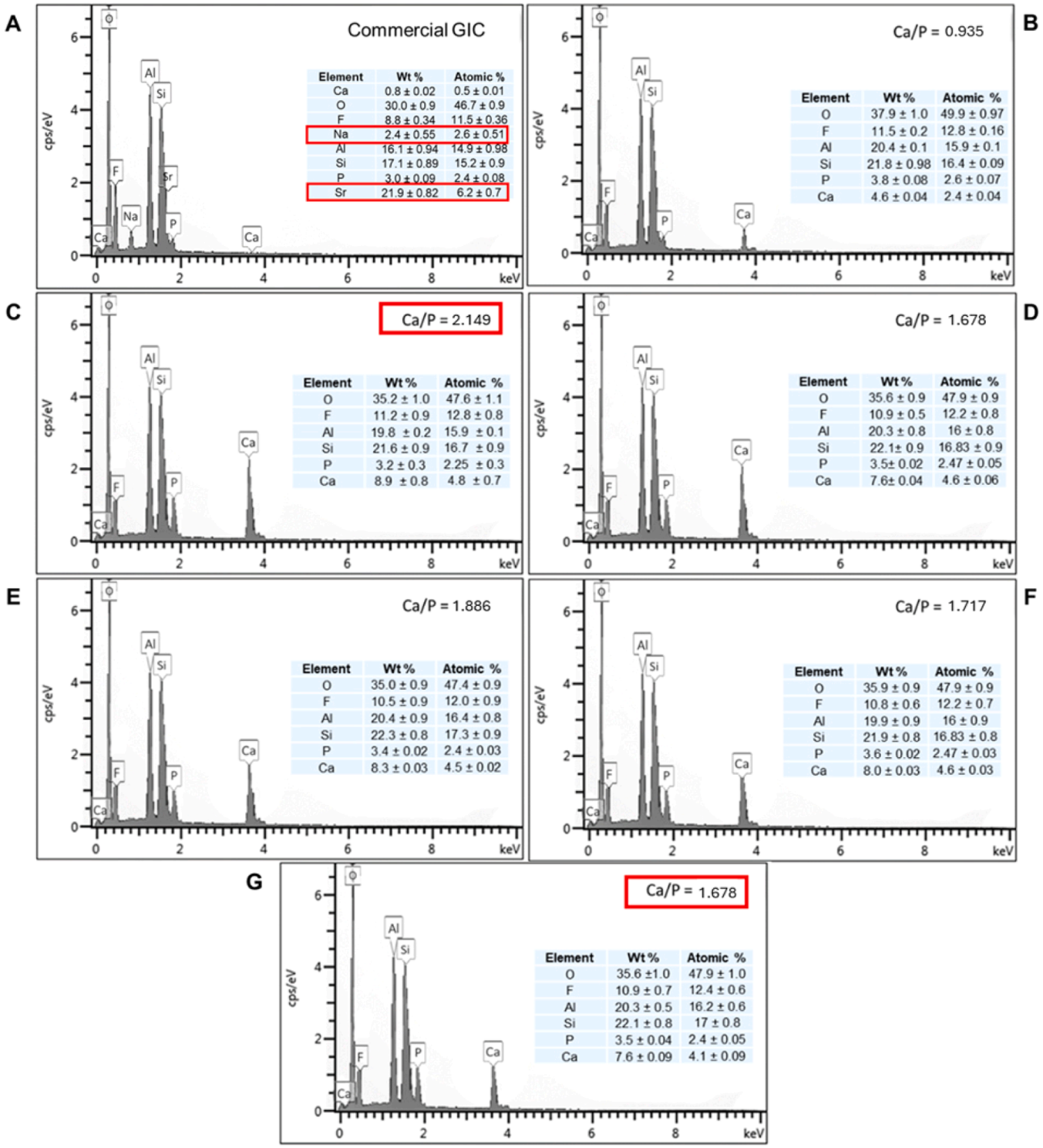

Fig. 2. Energy dispersive X-ray spectrum based on respective group: (A) Group A, (B) Group B, (C) Group C, (D) Group D, (E) Group E, (F) Group F and (G) Group G.

version 26.0 (IBM Corp., Armonk, NY, USA). One-way ANOVA (Analysis of Variance) was performed for the evaluation of initial setting time and compressive strength test, while detection of released ions (i.e., F, Ca, P) and pH measurements was measured using repeated measures ANOVA. For post-hoc analysis, Mauchly's test of sphericity was carried out to determine the relevant post-hoc test (Tukey HSD / Dunnett T3) based on the significance level.

3. Results

3.1. PSD data

Upon melting and crushing the chemical compounds, the resulting powder exhibited an average PSD of 1855 nm with 100 % homogeneity (Fig. 1A). Following the first step of ball milling, the PSD of the power was reduced. The major peak, representing 90.7 % of total samples, had an average PSD of 224.22 nm, whereas the minor peak accounting for the remaining total samples (9.3 %), had an average PSD of 702.4 nm (Fig. 1B).

To reduce the particle size, the second step of ball milling was executed. As results, an averaged PSD of 92.2 ± 2.69 nm demonstrating 100 % homogeneity was found (Fig. 1D, 1E, 1F). In contrast, Group A (control group) exhibited an average PSD of 769.3 nm with 100 % homogeneity (Fig. 1C).

Further analysis using FE-SEM revealed that the commercial GIC powder (683.75 ± 78.88 nm) demonstrated a higher average PSD compared to the fabricated GIC powder (80.0 ± 6.32 nm), as shown in Fig. 1H and 1G, respectively.

3.2. EDX data

Fig. 2A-2G show EDX spectrums in seven groups tested in this study. Of six groups (Groups B-G) of the facbricated GIC powder, Group C (2.1) exhibited a higher Ca/P ratio, followed by Groups E (1.88), D (1.86), F (1.73), and G (1.70). Meanwhile, the least Ca/P ration was observed in Group B (0.9). Although Ca/P ratio was highest in Group C, the mean ± SD atomic percentage of phosphorus (2.25 ± 0.3) in this group was the lowest compared to other groups. In contrast, the highest mean ± SD atomic percentage of phosphorus was found in Group B (2.6 ± 0.07).

For the EDX analysis, three spots on each sample were examined using consistent parameters, including magnifications, accelerating voltage, working distance, and count time. Notably, the fabricated GIC showed a higher concentration of calcium compared to the commercial variant (Fig. 2A and Fig. 2B).

The distribution of P and Ca displayed notable variations between the two groups. Group C (10 % TTCP; 0 % HAP): the Ca/P ratio was found to be approximately 2.1. This higher ratio is consistent with the inherent composition of TTCP, which is known to have a higher Ca/P

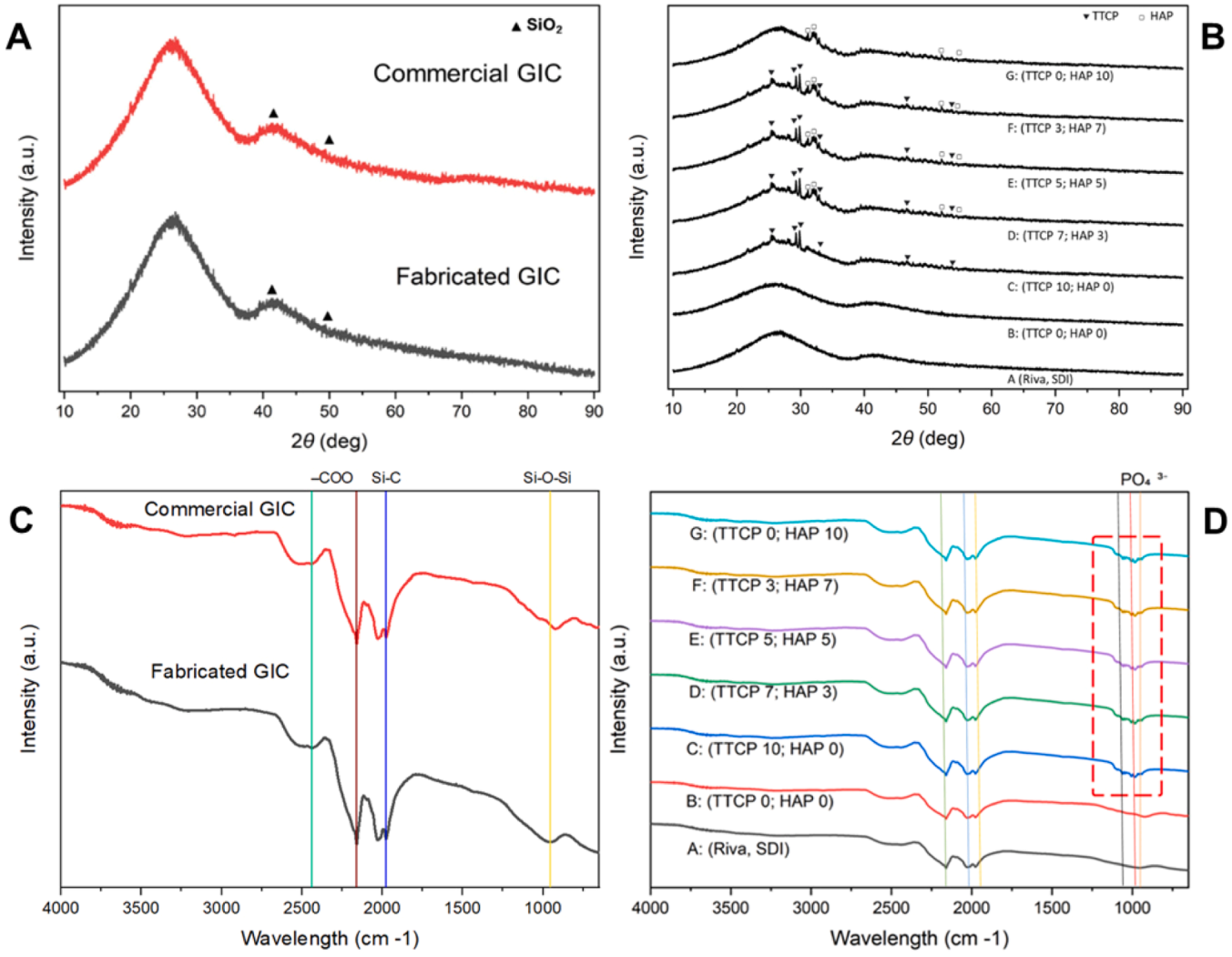

Fig. 3. (A) XRD patterns of commercial and fabricated GIC powders, (B) XRD patterns of seven groups, (C) FTIR spectral band of commercial and fabricated GIC powders, (D) FTIR spectral bands in seven groups.

ratio.

On the other hand, Group G (0 % TTCP; 10 % HAP) demonstrated a Ca/P ratio of approximately 1.7. This lower ratio aligns with the typical Ca/P ratio observed in hydroxyapatite. This lower ratio aligns with the typical Ca/P ratio observed in hydroxyapatite. The observed differences in the Ca/P ratios between the TTCP and HAP groups can be attributed to the intrinsic chemical compositions of TTCP and HAP. TTCP inherently possesses a higher Ca/P ratio than HAP, reflected in the EDX analysis results.

3.3. XRD and FTIR

Fig. 3A showed characteristic peaks of SiO_2 (silicon dioxide) (International Centre for Diffraction Data, ICDD 01-075-3169) of commercial and fabricated GIC powder in 2θ of 41.9° and 49.5°.

It was confirmed that the presence of both TTCP and HAP in the samples, as assessed by XRD patterns (Fig. 3B). Five groups (C, D, E, F and G) showed characteristic peaks of HAP (ICDD 00-009-0432) at 2θ values of 31.8, 32.9, 52.1, 54.4, and 78.1. Meanwhile, four groups showed characteristic peaks of TTCP (ICDD 01-084-9872) at 2θ values of 25.4, 29.2, 46.6, and 46.9.

Fig. 3C illustrates the FTIR spectrum in both commercial and fabricated GIC powders. By referring to Fig. 3C, Si-O-Si bending vibrational bonds was detected at ~ 950 cm^{-1}, while Si-C bond was discovered at ~ 1980 cm^{-1}. Besides, the presence of the FTIR spectral band at wavenumbers ~ 1980 and 2440 cm^{-1} represented the vibrational mode of the surface–COO group.

The FTIR spectral band generated from seven groups can be seen in Fig. 3D. As results, the existence of FTIR spectral band at ~ 875 cm^{-1} indicated the presence of TTCP and HAP via the detection of phosphate ion (HPO_4^{2-}). In addition, distinct absorption peaks were identified at ~ 2159, 2028, and 1976 cm^{-1}, corresponding to stretching vibrations of C≡C and C≡N groups, which are likely associated with trace organic impurities. Besides, absorption peaks at ~ 1057, 1044, 1004, and 983 cm^{-1} were associated with stretching vibrations of Si–O and P–O bonds, with the former and the latter was characterized as glass matrix and phosphate groups, respectively. The presence of absorption peak at ~ 940 cm^{-1} represented Si–O–Si bending vibrational bonds was further confrimed the structural characteristics of the fabricated materials.

3.4. Compressive strength

The results of the compressive strength test in the seven groups are displayed in Fig. 4. The fabricated GIC powder groups (Groups B-G) showed lower compressive strength when compared to the control group (Group A), with a significant difference was found across the experimental groups. Further analysis using Tukey's HSD post-hoc test revealed that Groups F (102.12 ± 2.85 MPa) and G (112.25 ± 4.80 MPa) was significantly increased compressive strength compared to Group A (131.74 ± 5.76 MPa) ($p < 0.05$), while Groups C (77.20 ± 2.49 MPa) and D (86.28 ± 2.66 MPa) were significantly reduced compressive strength compared to Group A ($p < 0.05$).

3.5. Initial setting time

By referring to Fig. 5, Group C (570 s) had recorded the longest setting time, followed by Groups D (543 s), E (523 s), G (422 s), F (416 s), and B (399 s) and the shortest setting time was observed in Group A (271 s). In addition, the results of an initial setting time discovered that Groups C (GIC-added 10 % TTCP), D (GIC-added 7 % TTCP), and E (GIC-added 5 % TTCP) exhibited an extension of initial setting time by 570, 543, and 523 s, respectively. On the contrary, both Groups F (GIC-added 7 % HAP) and G (GIC-added 10 % HAP) demonstrated a reduction of initial setting times by 416 s and 422 s each.

3.6. pH measurement

It was discovered that over time, except Group A, pH values showed a significant decline at time intervals of 1, 3, 6, and 12 hrs, followed by a significant increase at time intervals of 1, 3, 7, 14, and 28 days. The highest pH change was observed in Group C, from 6.73 ± 0.05 at 14 days to 6.93 ± 0.05 at 28 days.

All fabricated materials followed a consistent trend, shifting from acidic to a more neutral pH. Group A (Riva, SDI) started with the lowest pH and showed a significant increase of about 5.7 units, reaching a higher final pH. The largest pH shift was observed in Group C (10 % TTCP, 0 % HAP), reaching a pH of 6.9. By the end of the observation, the pH levels ranked from highest to lowest increase as follows: C (TTCP 10 %, HAP 0 %) > B (TTCP 0 %, HAP 0 %) > D (TTCP 7 %, HAP 3 %) > E (TTCP 5 %, HAP 5 %) > F (TTCP 3 %, HAP 7 %) > G (TTCP 0 %, HAP 10 %) > A (Riva, SDI). Changes in different time points are shown in Fig. 6 and statistical differences between the groups provided as a

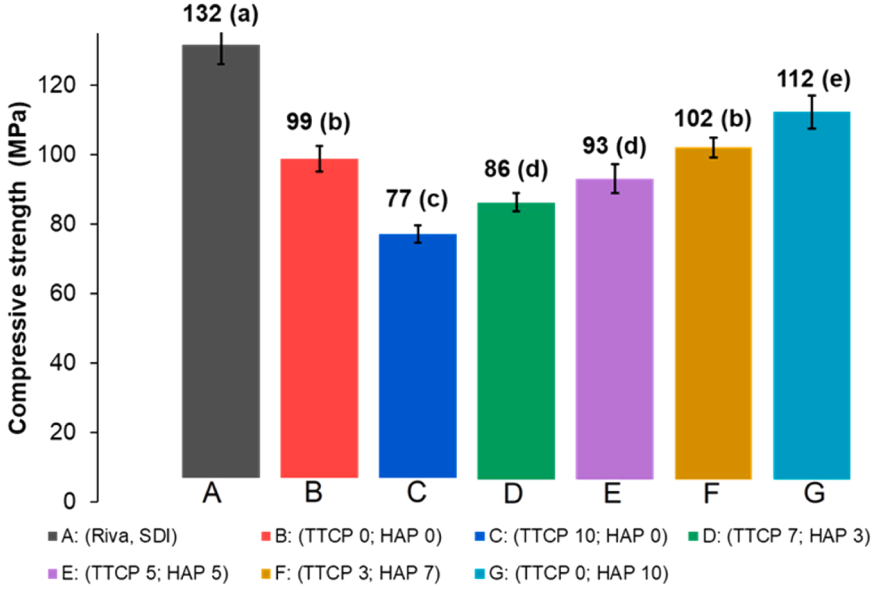

Fig. 4. Compressive strength analysis in seven different groups.

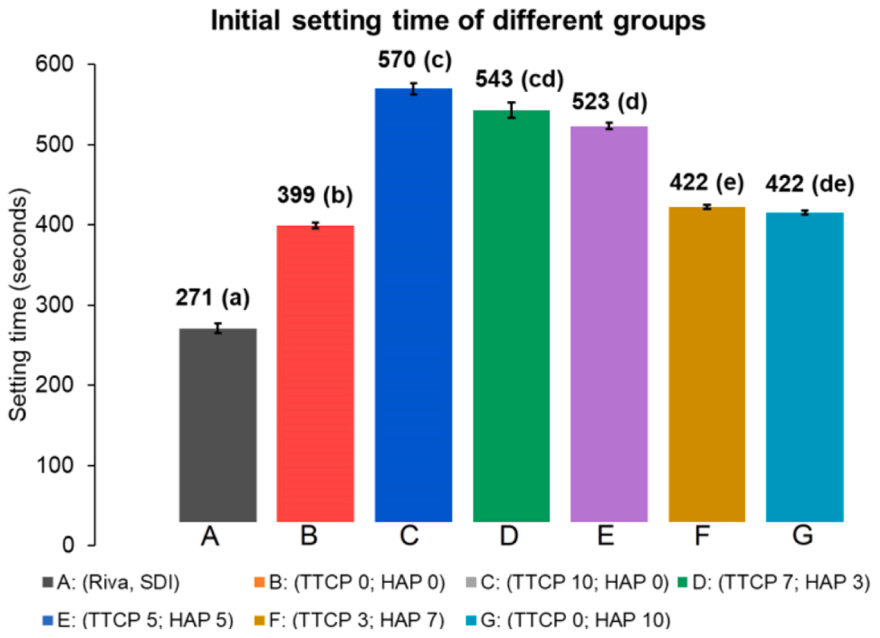

Fig. 5. Initial setting time of different groups. Different letters show significant differences between the groups using one-way ANOVA and Tukey HSD post-hoc testing. ($p < 0.05$).

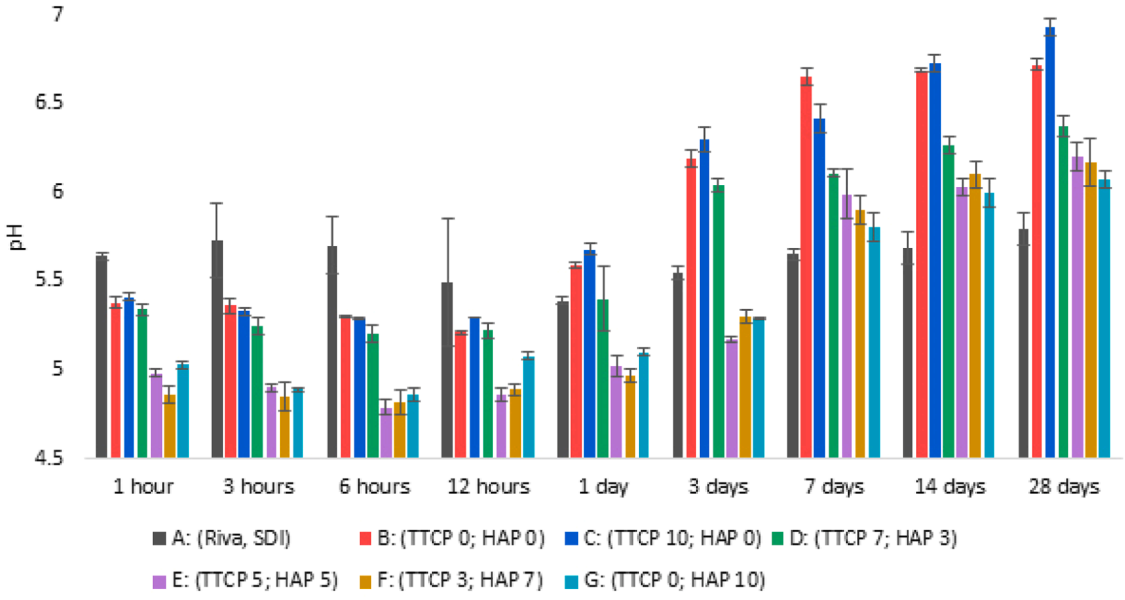

Fig. 6. Changes of the pH after soaking material in deionised water.

supplimentary data. Statistical differences between groups can be seen in Table 2.

3.7. Fluoride, calcium, and phosphate ions release

The fluoride ion release in seven groups at time intervals of 1, 3, 6, 12 hrs, 1, 3, 7, 14, and 28 days is illustrated in Fig. 7A and statistical differences between the groups provided as a supplimentary data. The control group (Group A) exhibited the highest fluoride ion release compared to the fabricated GIC groups (Groups B-G) across all time intervals, ranging from 5.39 ± 0.02 ppm to 5.79 ± 0.09 ppm. Besides, fluoride ion release showed a decreasing trend over time for all groups. Further result revealed that no significant difference between the control and other experimental groups was observed ($p < 0.05$). Statistical differences between groups can be seen in Table 3.

The phosphate ion release for fabricated GIC groups (Groups B-G) was significantly higher compared to the control group (Group A) (Fig. 7B), with the highest phosphate ion release over time intervals was found in Group C, ranging from 2.43 ± 0.05 ppm to 3.27 ± 0.19 ppm. Statistical differences between groups can be seen in Table 4.

The results also showed that variations of calcium ion release were influenced by the concentration of TTCP and HAP (Fig. 7C). Group C (TTCP: 10 %, HAP: 0 %) demonstrated the highest calcium ion release over time for all groups, ranging from 2.17 ± 0.54 ppm to 3.27 ± 0.19 ppm. At the study's endpoint, this group reached a maximum calcium leaching value of 2.4 parts per million (ppm). In contrast, Group A (control group) exhibited the lowest calcium ion release across time intervals, with the range of 0.17 ± 0.09 ppm to 1.20 ± 0.08 ppm.

Table 2
Statistical difference between groups for pH changes.

Groups*		1 hour**	3 hours**	6 hours**	12 hours**	1 day**	3 days**	7 days**	14 days**	28 days**
A: (Riva, SDI) (a)	Mean	5.64 (a)	5.73 (a)	5.70 (b)	5.49 (abc)	5.39 (dce)	5.55 (cef)	5.65 (efgh)	5.69 (fgh)	5.79 (hf)
	SD	0.02	0.21	0.16	0.36	0.02	0.04	0.03	0.09	0.09
B: (TTCP 0; HAP 0) (b)	Mean	5.38 (a)	5.36 (a)	5.30 (bcd)	5.21 (ce)	5.59 (defh)	6.19 (efgh)	6.65 (fgh)	6.69 (gh)	6.72 (h)
	SD	0.03	0.04	0.01	0.01	0.02	0.05	0.05	0.01	0.03
C: (TTCP 10; HAP 0) (b)	Mean	5.41 (a)	5.33 (abcdef)	5.29 (a)	5.30 (abc)	5.68 (bc)	6.30 (cdeg)	6.42 (def)	6.73 (ef)	6.93 (fg)
	SD	0.02	0.02	0.01	0.00	0.03	0.07	0.08	0.05	0.05
D: (TTCP 7; HAP 3) (b)	Mean	5.34 (a)	5.25 (a)	5.20 (ab)	5.22 (bc)	5.40 (cdh)	6.04 (defg)	6.11 (ehfg)	6.27 (fg)	6.37 (g)
	SD	0.03	0.05	0.05	0.04	0.18	0.04	0.02	0.05	0.06
E: (TTCP 5; HAP 5) (c)	Mean	4.98 (a)	4.90 (abh)	4.79 (a)	4.86 (abcd)	5.02 (chd)	5.17 (defg)	5.99 (e)	6.03 (fge)	6.20 (ge)
	SD	0.02	0.02	0.04	0.04	0.06	0.02	0.14	0.05	0.08
F: (TTCP 3; HAP 7) (d)	Mean	4.86 (a)	4.85 (a)	4.82 (adef)	4.89 (ac)	4.97 (bc)	5.30 (cde)	5.90 (def)	6.10 (ef)	6.17 (f)
	SD	0.05	0.08	0.07	0.03	0.04	0.04	0.08	0.08	0.13
G: (TTCP 0; HAP 10) (c)	Mean	5.03 (a)	4.89 (a)	4.86 (ab)	5.08 (a)	5.10 (bcdef)	5.29 (cdef)	5.81 (def)	6.00 (ef)	6.07 (f)
	SD	0.02	0.01	0.04	0.02	0.02	0.01	0.08	0.08	0.05

Different letters show significant differences between the groups.
* Statistical difference between intra groups has been assessed using Dunnett T3 Post Hoc test ($p < 0.05$)
** Statistical difference between inter groups has been assessed using the Pairwise Comparisons test ($p < 0.05$)

Statistical differences between groups can be seen in Table 5.

4. Discussion

GICs are not classified by particle size; the variation in the size of the glass powder used is a critical factor influencing their properties and clinical efficacy. A more profound comprehension of this aspect can contribute to the formulation of more specialized and efficacious GICs tailored for various dental applications. Research by De Caluwé et al. [26] indicated a significant effect of particle size on the properties of GICs, with the potential to enhance their mechanical properties.

Commercial and Fabricated GICs exhibited distinct chemical compositions, as confirmed by EDX. While the specific values varied, both GICs were predominantly composed of Al, Si, F, Ca, and P. In the case of Fuji IX GP Fast, as characterized by Yap et al. [27], the EDX analysis revealed that the three primary elements present were oxygen (66.75 %), silicon (13.18 %), and aluminum (12.82 %). Similarly, Fuji IX GP showed the same three main elements in its composition: oxygen (64.42 %), silicon (16.77 %), and aluminum (16.72 %).

The setting process of conventional GIC involves a sequence of stages through an acid-base reaction [28]. Prolonged initial setting time can be caused by the chemical properties of TTCP, particularly its higher solubility compared to other calcium phosphates, which results in a slower rate of the acid-base reaction that is fundamental to the setting process [29]. Additionally, the hydration process in TTCP is more complex and less efficient than in other calcium phosphate compounds, further contributing to the delay in setting [13,30,31].

The initial acidic nature of freshly mixed GIC, with a pH ranging between 0.9 and 1.6, has been frequently cited by researchers as a potential factor contributing to secondary caries in dental materials [32]. However, it is noteworthy that dentine can function as a buffer, and even thin layers of dentine existing between the restoration and the pulp can effectively prevent a significant reduction in pH impacting the pulp tissue. While several researchers have observed mild inflammatory responses, this response tends to be transient, resolving within 10–20 days as the pH increases within the first hour [33]. This behavior is attributed to the release of unreacted acrylic (or another organic acid) and its calcium salt, which acts as a weak acid and its conjugate base, forming a typical chemical buffer. Some researchers propose that this phenomenon may result from binding acid groups to polymer molecules with limited diffusivity [34].

Both TTCP and HAP shifted GICs toward near-neutral pH (~6.9), a profile associated with improved pulp compatibility but potentially interacting with early acid–base kinetics and initial strength development [28,35]. TTCP-rich groups in our study produced the greatest pH rise and showed sustained Ca^{2+}/PO_4^{3-} release across 28 days—consistent with recent evidence that Ca/PO_4-releasing modifications enhance bioactivity and remineralization—yet incurred prolonged setting and lower compressive strength, indicating a bioactivity–mechanics trade-off [5]. By contrast, HAP-rich GICs prioritized mechanical reinforcement and faster set with comparatively lower Ca^{2+} throughput, aligning with reports of nano-HAP additions improving compressive behavior [16]. Fluoride kinetics (day-1 peak, gradual decline) remained characteristic of conventional GICs and comparable to modified systems, indicating preserved fluoride-reservoir behavior [26,35]. The literature support an indication-specific approach: TTCP-rich GICs for liners/bases and non–load-bearing sites where sustained Ca/PO_4 release and pH buffering are paramount, and HAP-rich GICs for higher-load restorations where strength and handling dominate [26,28].

Group C (10 % TTCP; 0 % HAP) had a higher Ca/P ratio (2.1), while Group G (0 % TTCP; 10 % HAP) had a lower ratio (1.7). This difference reflects the inherent Ca/P ratios of the materials, with HAP at ~1.67 and TTCP at 2, as confirmed by EDX analysis [36]. Both TTCP and HAP incorporated in GICs lead to a sustained release of calcium and phosphate ions. These ions can help in buffering the acidic environment, gradually moving it towards neutrality [37,38]. This is particularly important in dental applications where a neutral pH is beneficial for tooth structure and health [39].

The fluoride release process is intricate and influenced by several intrinsic and environmental factors, including the organic matrix and filler composition, manipulation method, solubility, mass porosity, surface area, and pH. Across all examined samples, the maximum fluoride release occurred on the first day, followed by a gradual decrease in release up to the 28th day [40]. While extensive research has explored fluoride's anticaries effect, a thorough literature review did not yield specific data on the minimum fluoride release required to inhibit secondary caries [41]. Hicks et al. have reported that concentrations below 1 ppm of fluoride are adequate to diminish demineralization and enhance remineralization [42].

When GIC, incorporated by TTCP and HAP, is placed in an aqueous

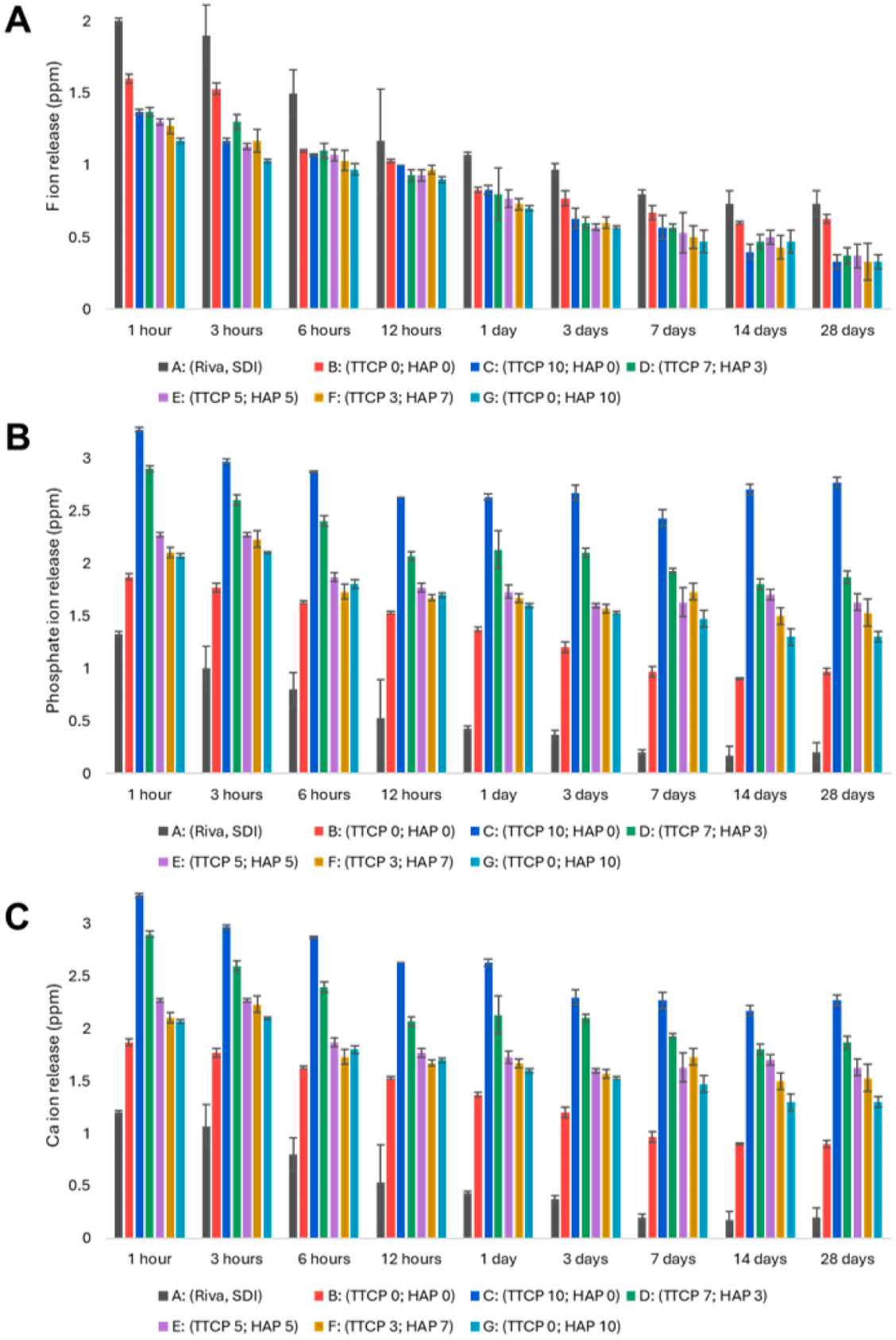

Fig. 7. A: Fluoride ion release (ppm) over time; B: Phosphate ion release (ppm) over time; C: Calcium ion release (ppm) over time.

Table 3
Statistical difference between groups for F ion release.

Groups*		1 hour**	3 hours**	6 hours**	12 hours**	1 day**	3 days**	7 days**	14 days**	28 days**
A: (Riva, SDI) (a)	Mean	2.00 (a)	1.90 (b)	1.50 (c)	1.17 (def)	1.07 (ef)	0.97 (fghj)	0.80 (gehj)	0.73 (hj)	0.73 (j)
	SD	0.08	0.08	0.08	0.05	0.05	0.05	0.08	0.05	0.05
B: (TTCP 0; HAP 0) (b)	Mean	1.60 (a)	1.53 (a)	1.10 (bc)	1.03 (ce)	0.83 (defh)	0.77 (efgh)	0.67 (fgh)	0.60 (gh)	0.63 (h)
	SD	0.08	0.05	0.08	0.05	0.05	0.05	0.12	0.08	0.12
C: (TTCP 10; HAP 0) (b)	Mean	1.37 (a)	1.17 (a)	1.07 (a)	1.00 (ab)	0.83 (cbg)	0.63 (cdef)	0.57 (dgef)	0.40 (ef)	0.33 (f)
	SD	0.12	0.09	0.09	0.08	0.05	0.05	0.09	0.08	0.05
D: (TTCP 7; HAP 3) (b)	Mean	1.37 (a)	1.30 (a)	1.10 (ab)	0.93 (bhc)	0.80 (cd)	0.60 (defg)	0.57 (efg)	0.47 (fg)	0.37 (g)
	SD	0.17	0.16	0.08	0.05	0.00	0.08	0.05	0.05	0.05
E: (TTCP 5; HAP 5) (c)	Mean	1.30 (a)	1.13 (a)	1.07 (a)	0.93 (ad)	0.77 (dc)	0.57 (cdef)	0.53 (def)	0.50 (ef)	0.37 (f)
	SD	0.08	0.05	0.05	0.05	0.05	0.09	0.05	0.00	0.05
F: (TTCP 3; HAP 7) (d)	Mean	1.27 (a)	1.17 (a)	1.03 (a)	0.97 (a)	0.73 (bc)	0.60 (cde)	0.50 (def)	0.43 (ef)	0.33 (f)
	SD	0.17	0.12	0.12	0.05	0.05	0.16	0.00	0.05	0.05
G: (TTCP 0; HAP 10) (c)	Mean	1.17 (a)	1.03 (a)	0.97 (a)	0.90 (a)	0.70 (bc)	0.57 (cdef)	0.47 (def)	0.47 (ef)	0.33 (f)
	SD	0.05	0.09	0.12	0.08	0.08	0.05	0.05	0.05	0.05

Different letters show significant differences between the groups.
* Statistical difference between intra groups has been assessed using Dunnett T3 Post Hoc test ($p < 0.05$)
** Statistical difference between inter groups has been assessed using the Pairwise Comparisons test ($p < 0.05$)

Table 4
Statistical difference between groups for P ion release.

Groups*		1 hour**	3 hours**	6 hours**	12 hours**	1 day**	3 days**	7 days**	14 days**	28 days**
A: (Riva, SDI) (ae)	Mean	1.33 (a)	1.00 (abcd)	0.80 (abcdefg)	0.53 (bcdefg)	0.43 (bcdefg)	0.37 (bcdefg)	0.20 (cdefg)	0.17 (cdefg)	0.20 (cdefg)
	SD	0.05	0.08	0.08	0.05	0.05	0.05	0.08	0.09	0.08
B: (TTCP 0; HAP 0) (aef)	Mean	1.87 (a)	1.77 (a)	1.63 (abcd)	1.53 (abcd)	1.37 (abd)	1.20 (abcd)	0.97 (bcd)	0.90 (cd)	0.97 (d)
	SD	0.17	0.05	0.09	0.05	0.17	0.14	0.21	0.16	0.09
C: (TTCP 10; HAP 0) (b)	Mean	3.27 (a)	2.97 (ab)	2.87 (ab)	2.63 (ab)	2.63 (ab)	2.67 (ab)	2.43 (b)	2.70 (ab)	2.77 (ab)
	SD	0.19	0.12	0.19	0.19	0.12	0.17	0.05	0.22	0.21
D: (TTCP 7; HAP 3) (bcf)	Mean	2.90 (a)	2.60 (abc)	2.40 (abcde)	2.07 (bcde)	2.13 (abcde)	2.10 (abcde)	1.93 (bcde)	1.80 (de)	1.87 (e)
	SD	0.33	0.14	0.37	0.57	0.39	0.36	0.33	0.28	0.05
E: (TTCP 5; HAP 5) (bcf)	Mean	2.27 (ab)	2.27 (b)	1.87 (ab)	1.77 (ab)	1.73 (ab)	1.60 (ab)	1.63 (ab)	1.70 (ab)	1.63 (a)
	SD	0.21	0.21	0.12	0.46	0.33	0.36	0.26	0.33	0.19
F: (TTCP 3; HAP 7) (bcf)	Mean	2.10 (abc)	2.23 (a)	1.73 (abc)	1.67 (abc)	1.67 (abc)	1.57 (abc)	1.73 (abc)	1.50 (b)	1.53 (c)
	SD	0.14	0.17	0.31	0.33	0.39	0.38	0.25	0.43	0.26
G: (TTCP 0; HAP 10) (dcf)	Mean	2.07 (a)	2.10 (a)	1.80 (abc)	1.70 (abc)	1.60 (abc)	1.53 (abc)	1.47 (abc)	1.30 (b)	1.30 (c)
	SD	0.17	0.14	0.22	0.37	0.28	0.33	0.41	0.16	0.08

Different letters show significant differences between the groups;
* Statistical difference between intra groups has been assessed using Tukey HSD Post Hoc test ($p < 0.05$)
** Statistical difference between inter groups has been assessed using the Pairwise Comparisons test ($p < 0.05$)

Table 5
Statistical difference between groups for Ca ion release.

Groups*		1 hour**	3 hours**	6 hours**	12 hours**	1 day**	3 days**	7 days**	14 days**	28 days**
A: (Riva, SDI) (a)	Mean	1.20 (a)	1.07 (a)	0.80 (abcde)	0.53 (abcde)	0.43 (abcd)	0.37 (abcd)	0.20 (be)	0.17 (ce)	0.20 (de)
	SD	0.08	0.05	0.08	0.05	0.05	0.05	0.08	0.09	0.08
B: (TTCP 0; HAP 0) (b)	Mean	1.87 (a)	1.77 (abc)	1.63 (ab)	1.53 (abcd)	1.37 (abcd)	1.20 (abcd)	0.97 (bcd)	0.90 (c)	0.90 (d)
	SD	0.17	0.05	0.09	0.05	0.17	0.14	0.21	0.16	0.16
C: (TTCP 10; HAP 0) (b)	Mean	3.27 (a)	2.97 (abcd)	2.87 (abcd)	2.63 (abcd)	2.63 (abcd)	2.30 (abcd)	2.27 (bcd)	2.17 (bcd)	2.27 (bcd)
	SD	0.19	0.12	0.19	0.19	0.12	0.65	0.19	0.54	0.56
D: (TTCP 7; HAP 3) (b)	Mean	2.90 (a)	2.60 (abcde)	2.40 (abcde)	2.07 (bcde)	2.13 (abcde)	2.10 (abcde)	1.93 (cbde)	1.80 (cbde)	1.87 (cbde)
	SD	0.33	0.14	0.37	0.57	0.39	0.36	0.33	0.28	0.05
E: (TTCP 5; HAP 5) (c)	Mean	2.27 (a)	2.27 (a)	1.87 (a)	1.77 (a)	1.73 (a)	1.60 (a)	1.63 (a)	1.70 (a)	1.63 (a)
	SD	0.21	0.21	0.12	0.46	0.33	0.36	0.26	0.33	0.19
F: (TTCP 3; HAP 7) (d)	Mean	2.10 (a)	2.23 (a)	1.73 (a)	1.67 (a)	1.67 (a)	1.57 (a)	1.73 (a)	1.50 (a)	1.53 (a)
	SD	0.14	0.17	0.31	0.33	0.39	0.38	0.25	0.43	0.26
G: (TTCP 0; HAP 10) (c)	Mean	2.07 (a)	2.10 (a)	1.80 (ab)	1.70 (ab)	1.60 (ab)	1.53 (ab)	1.47 (ab)	1.30 (ab)	1.30 (b)
	SD	0.17	0.14	0.22	0.37	0.28	0.33	0.41	0.16	0.08

Different letters show significant differences between the groups.
* Statistical difference between intra groups has been assessed using Tukey HSD Post Hoc test ($p < 0.05$)
** Statistical difference between inter groups has been assessed using the Pairwise Comparisons test ($p < 0.05$)

environment, its surface experiences continuous dissolution and precipitation due to ion transfer at the solid–liquid interface. This process results in a net release of calcium ions (Ca^{2+}) and phosphate ions (H_2PO^{4-}, HPO_3^{2-}, or PO_4^{3-}) from the material [43]. The extent of this behavior is influenced by factors such as crystal size, overall crystallinity, and the calcium-to-phosphate (Ca/P) ratio [44]. On the other

hand, the bioresorbability of TTCP results in a substantial release of calcium and phosphate ions [45]. This property is essential in dental applications where the restoration and maintenance of tooth mineral balance are necessary [46,47].

The relationship between the solubility of calcium phosphates and their mechanical strength can be explored. HAP, recognized for its low solubility and biocompatibility, emerged as a contributor to the mechanical strength of the modified nano-GIC formulations. The slow dissolution of HAP, consistent with its lower solubility compared to other calcium phosphates, provides sustained ion release without significantly compromising mechanical properties. The observed increase in compressive strength aligns with previous findings that highlight the reinforcing effect of hydroxyapatite on the mechanical integrity of dental materials [48].

It is important to acknowledge that the intrinsic mechanical characteristics of pure TTCP and HAP may influence the overall performance of the modified GICs. HAP, in its pure form, possesses a high modulus of elasticity, low solubility, and a stable crystalline hexagonal structure, which contributes to its known reinforcing effect when incorporated into composite materials [49,50]. This structural stability may have supported the observed enhancement in compressive strength in HAP-modified GIC groups (particularly Groups F and G), not solely due to chemical interaction with the GIC matrix but potentially also due to HAP's own mechanical contribution.

In contrast, TTCP has a higher solubility in aqueous environments and lower mechanical strength compared to HAP [49]. TTCP's dissolution and hydration can generate microstructural voids, reducing the continuity of the matrix. As TTCP degrades, it may create micro-defects and weaken the overall GIC matrix, introducing mechanical bias [51].

The enhanced hardness observed in the modified GIC with HAP may be attributed to the spherical GIC particles effectively filling voids within HAP particles and increasing the packing density in its matrix by occupying vacant spaces. The densely packed GIC matrix hinders the movement and merging of internal dislocations and defects, thereby resisting crack propagation. This mechanism aligns with findings in Moheet et al.'s study [52], where the addition of 10 % nano-HAP to GIC demonstrated superior mechanical strength.

Conversely, TTCP, characterized by its higher solubility, demonstrated a notable impact on ion release but was accompanied by a decreased compressive strength. This outcome corroborates with studies emphasising the trade-off between enhanced bioactivity, which is exemplified by increased ion release, and mechanical strength. The faster dissolution of TTCP, while promoting bioactivity, appears to compromise the reduction in compressive strength [53]. The decrease in mechanical strength of GIC modified with TTCP can indeed be associated with the bioresorbability of TTCP. As TTCP degrades, it can create micro-voids or structural weaknesses within the GIC matrix, which is responsible for the material's mechanical strength. When TTCP degrades, it may disrupt the matrix continuity, leading to reduced strength [45]. Looking ahead, AI-driven modeling and multi-objective optimization could predict formulation–property trade-offs (ion-release longevity vs. mechanical strength), guiding TTCP/HAP ratios that better balance bioactivity with load-bearing performance [54,55].

This study did not include microtensile/shear bond strength testing or interfacial analyses to confirm apatite interlayer formation; future work will evaluate these endpoints—after thermocycling and pH-cycling—to determine whether TTCP/HAP-induced ion release translates to clinically meaningful adhesion. All experiments were in vitro and did not simulate saliva, biofilm, or occlusal loading. Aging was limited to 28 days, and mechanical testing emphasized compressive strength and initial setting time rather than flexural/tensile strength, fracture toughness, wear, or fatigue. pH was measured in bulk solution rather than at the tooth–material interface, and the explored TTCP/HAP ratios may not capture the optimum composition. Clinical outcomes such as retention, marginal integrity, and postoperative sensitivity were not assessed, motivating future interfacial/bond testing and longer-term, clinically oriented evaluations.

5. Conclusions

This study demonstrated that the fabricated nano-sized GIC powder exhibited chemical variations and an amorphous phase, similar to commercial GIC. The incorporation of TTCP and HAP in the fabricated GIC formulation extended the setting time and significantly increased the release of calcium and phosphate ions, shifting the pH from acidic toward neutral. While HAP acted as a reinforcing agent by enhancing compressive strength, TTCP reduced mechanical strength. Only two of the fabricated groups achieved sufficient strength for restorative application as per ISO 9917-1:2007 requirements. These were Group F (TTCP 3 %; HAP 7 %) with a compressive strength of 102 MPa and Group G (TTCP 0 %; HAP 10 %) with 112 MPa; among them, Group G performed best. TTCP-modified GIC is more suitable for non-load-bearing restorations or cases where extended working time and ion release are prioritized, whereas HAP-modified GIC is recommended for load-bearing areas due to its superior strength and ion-releasing ability. Both formulations contribute to pH neutralization, making them especially advantageous for high-caries-risk patients and useful in preventive, pediatric, orthodontic, and restorative dentistry.

Declaration of generative AI and AI-assisted technologies in the writing process

During the preparation of this work, the authors used AI tools to improve readability and language. After using this tool/service, the authors reviewed and edited the content as needed and took full responsibility for the publication's content.

CRediT authorship contribution statement

Nozimjon Tuygunov: Writing – review & editing, Writing – original draft, Visualization, Validation, Investigation, Formal analysis, Data curation, Conceptualization. **Azwatee Abdul Aziz:** Writing – review & editing, Formal analysis. **Arief Cahyanto:** Writing – review & editing, Visualization, Validation, Methodology, Formal analysis. **Bakhtinur Khudanov:** Writing – review & editing, Validation, Investigation, Formal analysis, Data curation. **Muhammad Aidil Roslan:** Writing – review & editing, Investigation, Formal analysis, Data curation. **Zamri Radzi:** Writing – review & editing, Visualization, Validation, Supervision, Methodology, Formal analysis. **James Tsoi:** Writing – review & editing, Validation, Investigation, Formal analysis, Data curation. **Noor Azlin Yahya:** Writing – review & editing, Validation, Supervision, Investigation, Formal analysis.

Declaration of competing interest

The authors declare that they have no known competing financial interests or personal relationships that could have appeared to influence the work reported in this paper.

Acknowledgments

Not applicable.

References

[1] A. Moshaverinia, N. Roohpour, W.W.L. Chee, S.R. Schricker, A review of powder modifications in conventional glass-ionomer dental cements, J. Mater. Chem. 21 (5) (2011) 1319–1328, https://doi.org/10.1039/C0JM02309D.
[2] L. Samaranayake, T. Porntaveetus, J. Tsoi, N. Tuygunov, Facts and fallacies of the fluoride controversy: A contemporary perspective, Int. Dent. J. 75 (4) (2025) 100833, https://doi.org/10.1016/j.identj.2025.04.013.
[3] J. Makanjuola, S. Deb, Chemically activated glass-ionomer cements as bioactive materials in dentistry: A review, Prosthesis (2023) 327–345, https://doi.org/10.3390/prosthesis5010024.

[4] S. Chen, Y. Cai, H. Engqvist, W. Xia, Enhanced bioactivity of glass ionomer cement by incorporating calcium silicates, Biomatter. 6 (1) (2016) e1123842, https://doi.org/10.1080/21592535.2015.1123842.

[5] N. Tuygunov, Z. Khairunnisa, N.A. Yahya, A.A. Aziz, M.N. Zakaria, N.A. Israilova, A. Cahyanto, Bioactivity and remineralization potential of modified glass ionomer cement: A systematic review of the impact of calcium and phosphate ion release, Dent. Mater. J. advpub (2024), https://doi.org/10.4012/dmj.2023-132.

[6] T.P. Croll, J.W. Nicholson, Glass ionomer cements in pediatric dentistry: review of the literature, Pediatr. Dent. 24 (5) (2002) 423–429.

[7] J.F. Moraes, T. Gomes de Moraes, F.R.S. Nunes, E.M. Carvalho, G.S. Nunes, C. N. Carvalho, D.M. Ardenghi, J. Bauer, Formation of hydroxyapatite nanoprecursors by the addition of bioactive particles in resin-modified glass ionomer cements, Int. J. Adhes. Adhes. 110 (2021) 102933, https://doi.org/10.1016/j.ijadhadh.2021.102933.

[8] I. Antoniac, F. Miculescu, C. Cotrut, A. Ficai, J.V. Rau, E. Grosu, A. Antoniac, C. Tecu, I. Cristescu, Controlling the degradation rate of biodegradable Mg-Zn-Mn alloys for orthopedic applications by electrophoretic deposition of hydroxyapatite coating, Materials. (Basel) 13 (2) (2020), https://doi.org/10.3390/ma13020263.

[9] T. Salar, N. Tuygunov, N.A. Yahya, A.A. Aziz, The impact of resin coatings on the properties and performance of glass ionomer cements: A systematic review, J. Mech. Behav. Biomed. Mater. (2025) 107044, https://doi.org/10.1016/j.jmbbm.2025.107044.

[10] J. Sans, V. Sanz, J. Puiggalí, P. Turon, C. Alemán, Controlled anisotropic growth of hydroxyapatite by additive-free hydrothermal synthesis, Cryst. Growth Des. 21 (2) (2020) 748–756, https://doi.org/10.1021/acs.cgd.0c00850.

[11] B. Christie, N. Musri, N. Djustiana, V. Takarini, N. Tuygunov, M.N. Zakaria, A. Cahyanto, Advances and challenges in regenerative dentistry: A systematic review of calcium phosphate and silicate-based materials on human dental pulp stem cells, Mater. Today Bio 23 (2023) 100815, https://doi.org/10.1016/j.mtbio.2023.100815.

[12] M. Kheur, N. Kantharia, T. Lakha, S. Kheur, N. Al-Haj Husain, M. Özcan, Evaluation of mechanical and adhesion properties of glass ionomer cement incorporating nano-sized hydroxyapatite particles, Odontology 108 (1) (2020) 66–73, https://doi.org/10.1007/s10266-019-00427-5.

[13] C. Moseke, U. Gbureck, Tetracalcium phosphate: synthesis, properties and biomedical applications, Acta Biomater. 6 (10) (2010) 3815–3823, https://doi.org/10.1016/j.actbio.2010.04.020.

[14] Y. Yoshimine, K. Maeda, Histologic evaluation of tetracalcium phosphate-based cement as a direct pulp-capping agent, Oral Surg. Oral Med. Oral Pathol. Oral Radiol. 79 (3) (1995) 351–358, https://doi.org/10.1016/s1079-2104(05)80229-x.

[15] H.H. Xu, M.D. Weir, L. Sun, Calcium and phosphate ion releasing composite: effect of pH on release and mechanical properties, Dent. Mater. 25 (4) (2009) 535–542, https://doi.org/10.1016/j.dental.2008.10.009.

[16] A. Moshaverinia, S. Ansari, M. Moshaverinia, N. Roohpour, J.A. Darr, I. Rehman, Effects of incorporation of hydroxyapatite and fluoroapatite nanobioceramics into conventional glass ionomer cements (GIC), Acta Biomater. 4 (2) (2008) 432–440, https://doi.org/10.1016/j.actbio.2007.07.011.

[17] T. Qin, X. Li, H. Long, S. Bin, Y. Xu, Bioactive tetracalcium phosphate scaffolds fabricated by selective laser sintering for bone regeneration applications, Mater. (Basel) 13 (10) (2020), https://doi.org/10.3390/ma13102268.

[18] L.C. Chow, S. Takagi, R.J. Shern, T.H. Chow, K.K. Takagi, B.A. Sieck, Effects on whole saliva of chewing gums containing calcium phosphates, J. Dent. Res. 73 (1) (1994) 26–32, https://doi.org/10.1177/00220345940730010401.

[19] N.U. P, K.K. Srinivasan, A.V. Adhikari, L.N. Satapathy, Evaluation of calcium fluoroaluminosilicate based glass ionomer luting cements processed both by conventional and microwave assisted methods, Technologies (2015) 58–73, https://doi.org/10.3390/technologies3020058.

[20] N. Krajangta, C. Dulsamphan, T. Chotitanmapong, Effects of protective surface coating on fluoride release and recharge of recent uncoated high-viscosity glass ionomer cement, Dent. J. (Basel) 10 (12) (2022), https://doi.org/10.3390/dj10120233.

[21] H.S. Vilela, M.C.A. Resende, R.B. Trinca, T. Scaramucci, L.O. Sakae, R.R. Braga, Glass ionomer cement with calcium-releasing particles: effect on dentin mineral content and mechanical properties, Dent. Mater. 40 (2) (2024) 236–243, https://doi.org/10.1016/j.dental.2023.11.005.

[22] I.O.f. Standardization, Dentistry — Water-based cements — Part 1: Powder/liquid acid-base cements, ISO, 2007.

[23] A.J. Noori, F.A. Kareem, Setting time, mechanical and adhesive properties of magnesium oxide nanoparticles modified glass-ionomer cement, J. Mater. Res. Technol. 9 (2) (2020) 1809–1818, https://doi.org/10.1016/j.jmrt.2019.12.012.

[24] I.O.f. Standardization, ISO 9917-1: Dental water-based cements, ISO Geneva 2003.

[25] Y.-N. Jeong, S.-Y. Yang, B.-J. Park, Y.-J. Park, Y.-C. Hwang, I.-N. Hwang, W.-M. Oh, Physical and chemical properties of experimental mixture of mineral trioxide aggregate and glass ionomer cement, Restor. Dent. Endod. 35 (2010), https://doi.org/10.5395/JKACD.2010.35.5.344.

[26] T. De Caluwé, C.W. Vercruysse, S. Fraeyman, R.M. Verbeeck, The influence of particle size and fluorine content of aluminosilicate glass on the glass ionomer cement properties, Dental Mater. 30 (9) (2014) 1029–1038, https://doi.org/10.1016/j.dental.2014.06.003.

[27] A.U. Yap, Y.S. Pek, P. Cheang, Physico-mechanical properties of a fast-set highly viscous GIC restorative, J. Oral Rehabil. 30 (1) (2003) 1–8, https://doi.org/10.1046/j.1365-2842.2003.01006.x.

[28] M. Khoroushi, F. Keshani, A review of glass-ionomers: from conventional glass-ionomer to bioactive glass-ionomer, Dent. Res. J. (Isfahan) 10 (4) (2013) 411–420.

[29] H.B. Pan, B.W. Darvell, Solubility of TTCP and beta-TCP by solid titration, Arch. Oral Biol. 54 (7) (2009) 671–677, https://doi.org/10.1016/j.archoralbio.2008.01.001.

[30] M.M. Radwan, M.E. Khallaf, Hydration behavior of an experimental tricalcium silicate/tetracalcium phosphate bio-cement in Streptococcus thermophiles bacterial solution in comparison with distilled water used as a root canal furcation perforation repair material, Bull. Natl. Res. Centre 46 (1) (2022) 207, https://doi.org/10.1186/s42269-022-00889-8.

[31] Z. Khairunnisa, N. Tuygunov, A. Cahyanto, W.H. Aznita, I.A. Purwasena, N.S. M. Noor, N.H. Azami, M.N. Zakaria, Potential of microbial-derived biosurfactants for oral applications-a systematic review, BMC. Oral Health 24 (1) (2024) 707, https://doi.org/10.1186/s12903-024-04479-0.

[32] I. Nedeljkovic, J. De Munck, V. Slomka, B. Van Meerbeek, W. Teughels, K. Van Landuyt, Lack of buffering by composites promotes shift to more cariogenic bacteria, J. Dent. Res. 95 (8) (2016) 875–881, https://doi.org/10.1177/0022034516647677.

[33] M. Almuhaiza, Glass-ionomer cements in restorative dentistry: a critical appraisal, J. Contemp. Dent. Pract. 17 (4) (2016) 331–336, https://doi.org/10.5005/jp-journals-10024-1850.

[34] I. Nedeljkovic, J. De Munck, A. Vanloy, D. Declerck, P. Lambrechts, M. Peumans, W. Teughels, B. Van Meerbeek, K.L. Van Landuyt, Secondary caries: prevalence, characteristics, and approach, Clin. Oral Investig. 24 (2) (2020) 683–691, https://doi.org/10.1007/s00784-019-02894-0.

[35] S.K. Sidhu, J.W. Nicholson, A review of Glass-Ionomer cements for clinical dentistry, J. Funct. Biomater. 7 (3) (2016), https://doi.org/10.3390/jfb7030016.

[36] M.D. Vlad, S. Gómez, M. Barracó, J. López, E. Fernández, Effect of the calcium to phosphorus ratio on the setting properties of calcium phosphate bone cements, J. Mater. Sci. Mater. Med. 23 (9) (2012) 2081–2090, https://doi.org/10.1007/s10856-012-4686-3.

[37] A. Mocanu, O. Cadar, P.T. Frangopol, I. Petean, G. Tomoaia, G.-A. Paltinean, C. P. Racz, O. Horovitz, M. Tomoaia-Cotisel, Ion release from hydroxyapatite and substituted hydroxyapatites in different immersion liquids: *in vitro*experiments and theoretical modelling study, R. Soc. Open. Sci. 8 (1) (2021) 201785, https://doi.org/10.1098/rsos.201785.

[38] R. Jayasree, T.S. Sampath Kumar, G. Perumal, M. Doble, Drug and ion releasing tetracalcium phosphate based dual action cement for regenerative treatment of infected bone defects, Ceram. Int. 44 (8) (2018) 9227–9235, https://doi.org/10.1016/j.ceramint.2018.02.133.

[39] K. Yu, Q. Zhang, Z. Dai, M. Zhu, L. Xiao, Z. Zhao, Y. Bai, K. Zhang, Smart dental materials intelligently responding to oral pH to combat caries: A literature review, Polymers. (Basel) 15 (12) (2023) 2611, https://doi.org/10.3390/polym15122611.

[40] N.S. Al Ibrahim, J.F. Tahmassebi, K.J. Toumba, In Vitro and ln vivo assessment of newly developed slow-release fluoride glass device, Eur. Arch. Paediatr. Dent. 11 (3) (2010) 131–135, https://doi.org/10.1007/bf03262728.

[41] L. Forsten, Fluoride release and uptake by glass-ionomers and related materials and its clinical effect, Biomaterials 19 (6) (1998) 503–508, https://doi.org/10.1016/S0142-9612(97)00130-0.

[42] J. Hicks, F. Garcia-Godoy, C. Flaitz, Biological factors in dental caries: role of remineralization and fluoride in the dynamic process of demineralization and remineralization (part 3), J. Clin. Pediatr. Dent. 28 (3) (2008) 203–214, https://doi.org/10.17796/jcpd.28.3.w0610427l746j34n.

[43] L. Wang, G.H. Nancollas, Calcium orthophosphates: crystallization and dissolution, Chem. Rev. 108 (11) (2008) 4628–4669, https://doi.org/10.1021/cr0782574.

[44] M.C. Rodrigues, L.C. Natale, V.E. Arana-Chaves, R.R. Braga, Calcium and phosphate release from resin-based materials containing different calcium orthophosphate nanoparticles, J. Biomed. Mater. Res. B Appl. Biomater. 103 (8) (2015) 1670–1678, https://doi.org/10.1002/jbm.b.33327.

[45] C.H. Tsai, R.M. Lin, C.P. Ju, J.H. Chern Lin, Bioresorption behavior of tetracalcium phosphate-derived calcium phosphate cement implanted in femur of rabbits, Biomaterials 29 (8) (2008) 984–993, https://doi.org/10.1016/j.biomaterials.2007.10.014.

[46] N.J. Cochrane, F. Cai, N.L. Huq, M.F. Burrow, E.C. Reynolds, New approaches to enhanced remineralization of tooth enamel, J. Dent. Res. 89 (11) (2010) 1187–1197, https://doi.org/10.1177/0022034510376046.

[47] K.J. Cross, N.L. Huq, E.C. Reynolds, Casein phosphopeptides in oral health–chemistry and clinical applications, Curr. Pharm. Des. 13 (8) (2007) 793–800, https://doi.org/10.2174/138161207780363086.

[48] S. Suvarnapathaki, X. Wu, D. Lantigua, M.A. Nguyen, G. Camci-Unal, Hydroxyapatite-incorporated composite gels improve mechanical properties and bioactivity of bone scaffolds, Macromol. Biosci. 20 (10) (2020) e2000176, https://doi.org/10.1002/mabi.202000176.

[49] A.A. Mirtchi, J. Lemaître, E. Munting, Calcium phosphate cements: action of setting regulators on the properties of the beta-tricalcium phosphate-monocalcium phosphate cements, Biomaterials 10 (9) (1989) 634–638, https://doi.org/10.1016/0142-9612(89)90120-8.

[50] S. Dorozhkin, Calcium orthophosphates: applications in nature, biology, and medicine [Hardcover], 2012.

[51] J. Luo, I. Ajaxon, M.P. Ginebra, H. Engqvist, C. Persson, Compressive, diametral tensile and biaxial flexural strength of cutting-edge calcium phosphate cements, J. Mech. Behav. Biomed. Mater. 60 (2016) 617–627, https://doi.org/10.1016/j.jmbbm.2016.03.028.

[52] I.A. Moheet, N. Luddin, I. Ab Rahman, S.a.M. Masudi, T.P. Kannan, N.R.N. Abd Ghani, Evaluation of mechanical properties and bond strength of nano-hydroxyapatite-silica added glass ionomer cement, Ceram. Int. 44 (8) (2018) 9899–9906, https://doi.org/10.1016/j.ceramint.2018.03.010.

[53] J. Liu, J. Liao, Y. Li, Z. Yang, Q. Ying, Y. Xie, A. Zhou, Bioactive tetracalcium phosphate/magnesium phosphate composite bone cement for bone repair, J. Biomater. Appl. 34 (2) (2019) 239–249, https://doi.org/10.1177/0885328219845597.

[54] N. Tuygunov, L. Samaranayake, Z. Khurshid, P. Rewthamrongsris, F. Schwendicke, T. Osathanon, N.A. Yahya, The Transformative role of artificial intelligence in dentistry: A comprehensive overview part 2: the promise and perils, and the international dental federation Communique, Int. Dent. J. 75 (2) (2025) 397–404, https://doi.org/10.1016/j.identj.2025.02.006.

[55] L. Samaranayake, N. Tuygunov, F. Schwendicke, T. Osathanon, Z. Khurshid, S. A. Boymuradov, A. Cahyanto, The transformative role of artificial intelligence in dentistry: A comprehensive overview. Part 1: fundamentals of AI, and its contemporary applications in dentistry, Int. Dent. J. 75 (2) (2025) 383–396, https://doi.org/10.1016/j.identj.2025.02.005.